Proc. Natl. Acad. Sci. USA
Vol. 96, pp. 10854–10856, September 1999
Medical Sciences

Subsurface tumor progression investigated by noninvasive optical second harmonic tomography

(second harmonic generation/optical tomography/histology)

YICI GUO*, HOWARD E. SAVAGE†, FENG LIU*, STIMSON P. SCHANTZ†, P. P. HO*, AND R. R. ALFANO*‡

*Institute for Ultrafast Spectroscopy and Lasers, New York State Center for Advanced Technology for Ultrafast Photonic Materials and Applications and Department of Energy Center of Excellence in Laser Imaging and Cancer Diagnostics, Departments of Electrical Engineering and Physics, The City College and Graduate School of The City University of New York, New York, NY 10031; and †New York Eye and Ear Infirmary, Second Avenue at 14th Street, New York, NY 10003

Communicated by Melvin Lax, City College of the City University of New York, New York, NY, July 15, 1999 (received for review December 1, 1998)

ABSTRACT **Nonlinear optical imaging with femtosecond (10^{-15}-second) laser technology was used to evaluate the subsurface tumor progression in control, dysplasia, and cancerous 7,12-dimethylbenz[*a*]anthracene-treated hamster cheek pouch mucosa tissues. Two-dimensional images of hamster cheek pouch mucosa tissues were obtained by scanning the second harmonic signal at various sagittal and axial positions. The spatial mapping of the second harmonic signals showed depth differentiation between normal, dysplasia, and a more advanced cancerous state. This nonlinear optical method offers a noninvasive *in situ* imaging tool to the medical community.**

The medical community is searching for new and noninvasive *in situ* methods to better characterize the mucosal tissues of the cervix, colon, ear, nose, throat, oral cavity, and esophagus, where disease starts at the epithelial layer a few hundred micrometers beneath the surface. Second harmonic generation (SHG) imaging is a nonlinear optical technique that produces images of subsurface structures, rendering *in situ* histological information of tissues without surgery. The image-forming signal depends on the morphological symmetry of the molecules and the local intra- and intercellular matrices of the tissue. This symmetry dependence is derived from the second-order, nonlinear optical susceptibility χ^2 tensor component that has been used to study phenomena both in the interior region and at surfaces or interfaces in various materials, including biological samples (1–6).

SHG tomography can provide information about tissue structure in addition to that offered by other linear optical microscopy techniques, such as optical coherence tomography (OCT) and reflectance confocal microscopy (7, 8). Both of these latter methods depend on the reflectance changes caused by local variations in the indices of refraction. Imaging techniques such as ultrasound and MRI with surface coils (100-μm in spatial resolution) are limited in their ability to provide submicrometer resolutions that are comparable to linear and nonlinear optical microscopy (9,§). The application of localized excitation makes it possible to use optical sectioning and image mapping in evaluating tissue *in situ*. This nonlinear optical technique allows imaging that is not restricted to signals emitted from fluorescent molecules. The illumination needs not correspond to a particular absorption band of a molecule; the wavelength can be selected to optimize excitation and imaging conditions. The SHG signal is proportional to the reflective coefficient and dependent on the reciprocal of quadratic powers of the index of refraction (6). This useful property provides a higher optical contrast for visualizing matrix structures than does reflectance microscopy such as OCT, in which the signal is proportional to the reflective coefficients.

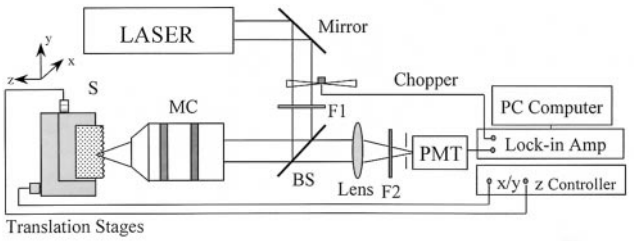

FIG. 1. Schematic diagram of experimental setup. BS, dichroic beam splitter; F1, long-pass ($\lambda > 760$ nm) filter; F2, short-pass and band-pass filter; MC, microscope objective; PMT, photomultiplier tube; S, sample.

In this report, we demonstrate the applicability of the SHG imaging technique for the evaluation of subsurface tumor progression from normal to advanced cancer states. This technology provides a noninvasive histological and medical diagnostic modality. Our studies were performed on hamster cheek pouch mucosal tissues.

MATERIALS AND METHODS

A schematic diagram of the optical experimental arrangement is shown in Fig. 1. A self mode-locked Ti:sapphire laser system, operating at a center wavelength of 800 nm, with a pulse duration of 120 fs (full width at half maximum or FWHM) and a pulse repetition rate of 76 MHz, was used as the excitation source. The output beam was passed through a long-pass filter ($\lambda > 760$ nm) and expanded through a series of lenses. The beam was reflected by a dichroic beam splitter and focused onto the specimen by a $\times 20$ microscope objective (numerical aperture = 0.4). The average power was approximately 80 mW at the sample site. The backscattered SHG light from the focal point of the sample was transmitted through the objective lens and the dichroic beam splitter, then focused by a lens onto a photomultiplier tube (PMT). A computer-controlled lock-in

The publication costs of this article were defrayed in part by page charge payment. This article must therefore be hereby marked "*advertisement*" in accordance with 18 U.S.C. §1734 solely to indicate this fact.

PNAS is available online at www.pnas.org.

Abbreviations: DMBA, 7,12-dimethylbenz[*a*]anthracene; OCT, optical coherence tomography; PMT, photomultiplier tube; SHG, second harmonic generation.

‡To whom reprint requests should be addressed at: Physics Department, Room J419, City College of New York, 138th Street and Convent Avenue, New York, NY 10031. E-mail: alfano@scisun.sci.ccny.cuny.edu.

§See Nakanishi, K., Nishii, T., Naito, H., Tamura, S. & Nakamura, H., *Proceedings of the International Symposium on Computer and Communication Systems for Image-Guided Diagnosis and Therapy*, pp. 139–142, June 1996, Paris.

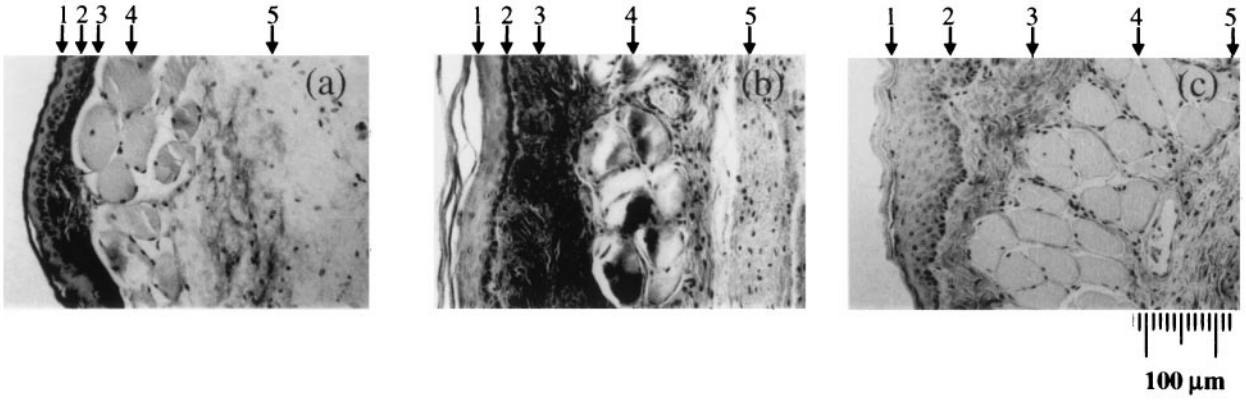

FIG. 2. Hematoxylin/eosin stains of crosssection of hamster cheek pouches. The five different distinct tissue layers are (*1*) the cornified cell surface layer; (*2*) a layer of flat stratified squamous epithelium without rete pegs, usually two to four cell layers thick; (*3*) a submucosa of dense fibrous connective tissue; (*4*) a layer of longitudinal striated muscle fiber; and (*5*) a layer of loose areolar connective tissue. (*a*) An 8-week saline-control animal. (*b*) An animal that had its cheek pouch painted with mineral oil containing 0.5% DMBA three times a week for 8 weeks. Note thickening of epithelial cell layer. (*c*) An animal that had its cheek pouch painted with mineral oil containing 0.5% DMBA three times a week for 14 weeks. Note thickening of epithelial cell layer.

amplifier was used to detect the signal from the PMT and to record the data. Two short band pass filters and a narrow band filter were placed in front of the PMT to isolate the SHG signal at 400 nm and reject scattered light at the fundamental wavelength.

The estimated rejection ratio at 800 nm from the dichroic beam splitter in conjunction with optical filters was approximately 1×10^9 to 1. The samples were continuously scanned along the axial depth (z axis) direction and along the transverse (y axis) direction with a 0.1-s integration time at each data point. The acquisition time for an image was approximately 30 min. The lateral and axial resolutions of the system were 5 μm and 40 μm, respectively.

The hamster cheek pouch carcinogenesis process was undertaken according to the methods developed by Salley (10). The hamster cheek pouches were painted thrice weekly with mineral oil containing 0.5% 7,12-dimethylbenz[*a*]anthracene (DMBA) or with mineral oil alone. Eight and 14 weeks after the first painting, the hamsters were killed by CO_2 asphyxiation; the cheek pouches were removed, cut down the midline, placed on filter paper with the lumen side up, and transferred to 10% buffered formalin for a minimum of 48 hr. Prior to optical analysis, the cheek pouch tissue was washed in 0.01 M phosphate-buffered saline solution at a pH of 7.0. One set of tissue samples was imaged with the SHG technique.

Salley (10) described in detail the histological changes in the hamster cheek pouch over time of DMBA treatment. The hamster cheek pouch has five distinct layers. Starting at the lumen surface and traversing through the pouch are: (*i*) the surface layer of cornified cells; (*ii*) an epithelial layer consisting of a basal cell layer of flat, stratified squamous epithelium without rete pegs, usually 2–4 cell layers thick, and a suprabasal layer that develops (up to 15–20 cell layers thick after 14 weeks) over the time of treatment with DMBA; (*iii*) a submucosa of dense fibrous connective tissue; (*iv*) a layer of longitudinal striated muscle fibers; and (*v*) a layer of loose areolar connective tissue.

The conventional histology of hamster cheek pouch tissues for staging the development of cancer under DMBA treatment is shown in Fig. 2. Fig. 2*a* shows a normal control tissue with the epithelium consisting of a suprabasal layer 2 cell layers thick and a basal cell layer. In Fig. 2*b*, the tissue shows the dysplastic characteristics; the suprabasal layer grows to 6 to 7 cell layers. At the more advanced cancerous stage, shown in Fig. 2c, the suprabasal layer extends to more than 10 cell layers thick.

RESULTS

Fig. 3 shows the two-dimensional second harmonic tomographic images of the control (*A*), 8-week (*B*), and 14-week (*C*) DMBA-treated hamster cheek pouch tissues. The tissues were used to evaluate the invasion depth of the respective tumor progression stages. The figure displays the two-dimensional lateral and depth (y and z) plane, color-coded SHG intensity images. The corresponding conventional histological images are shown in Fig. 2 *a–c*.

DISCUSSION

That the multiple layers or interfaces inside the tissue are visible in the SHG images (Fig. 3) is the result of the symmetry

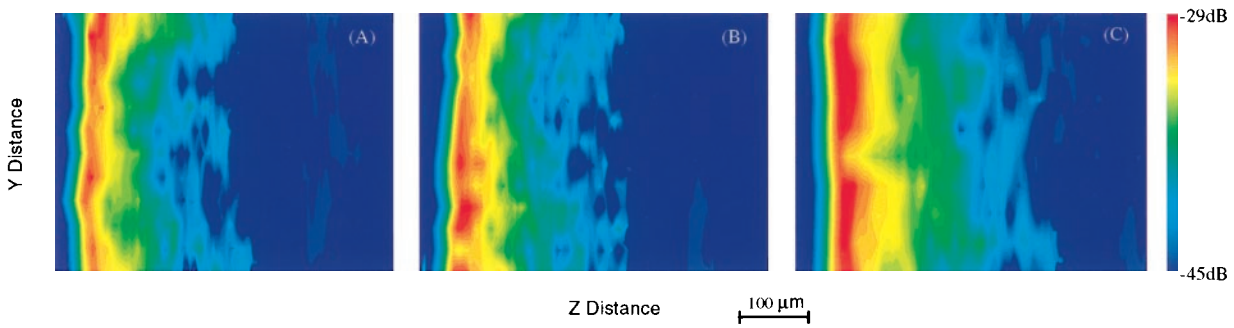

FIG. 3. Two-dimensional tomographic second harmonic images obtained by 120-fs laser pulse excitation at 800 nm. (*A*) Normal hamster pouch tissue. (*B*) Hamster pouch tissue after 8 weeks of carcinogen (DMBA) treatment. (*C*) Hamster pouch tissue after 14 weeks of carcinogen (DMBA) treatment.

dependence of the SHG signal on the tissue structure and on changes in local symmetry. The salient feature is the thickness of the various sublayers; they indicate the different stages of tumor progression. With increasing time of DMBA treatment, the cheek pouch progresses through distinct changes including hyperplasia, benign papilloma, squamous carcinoma *in situ*, and squamous cell carcinoma with both local invasion and metastasis. The layer most affected by this process is the epithelial layer. This layer increases in thickness over the treatment interval. The thickening is seen in both the histologic and the corresponding SHG images as the yellow and red regions.

Our results show the application of SHG tomography in evaluating tumor progression stages beneath the mucosal surface. The structural detail in the images, limited at the present time by the resolution of our imaging system, can be improved with higher numerical aperture objective lens. The progressive loss in signal intensity is primarily because of the scattering nature of the biological tissue. A tissue with a higher scattering coefficient would decrease the primary (pump) intensity significantly, compared with tissues that are less scattering. Because the second harmonic signal depends on the square of the pump intensity, SHG signals decrease faster than the linearly reflected light at the primary wavelength. The scattering strength of the epidermis is weaker than that of the dermis. In the visible and near-infrared spectral region (1,000 nm to 400 nm), the scattering coefficient of the human epidermis is less than half that of the dermis (11). This property helps SHG imaging through the thicker epidermis layers. The strength of the SHG signal depends on the local symmetry. For biological tissues, scattering strength lessens as the wavelength of light lengthens. By using longer wavelength light, such as $1300 \approx 1500$ nm light, it is possible to reduce the scattering loss of the SHG signal and to image deeper into the tissue. Scattering causes signal intensity loss and reduces the spatial confinement of the SHG signal. The detected SHG signal can include a significant contribution from nonfocal regions when the focal point is several scattering lengths inside the tissue (12). Further study of SHG light generation and its propagation in tissues is needed to obtain structural images deep inside tissues. Our SHG technique, unlike OCT and reflectance confocal microscopy, is a nonlinear optical process that is sensitive to the local symmetry and second order nonlinear susceptibility of the particular tissue.

The SHG imaging technique is well suited for *in vitro* and *in vivo* imaging of the early stages of diseases that appear first in the epithelial layer, such as diseases of the skin, oral cavity, throat, nose, ear, cervix, colon, and esophagus. With the scanning laser beam, three-dimensional subsurface structure of tissues can be imaged without surgery. Scanning imaging can also be implemented with fiber optics adapted for endoscopy evaluation. For *in vivo* clinical applications, the safety issues of high-peak-power laser pulses need to be investigated.

The use of SHG noninvasive technology to evaluate subsurface tumor progression stages without cutting into the tissue has been demonstrated. Second harmonic tomographic imaging in hamster cheek pouch tissues, including normal control, dysplasia, and cancer after 8 and 14 weeks of carcinogen treatment, shows the usefulness of *in situ* histology. With lateral and axial scanning, two-dimensional intensity maps were obtained that correlated SHG signal intensity with histological findings and showed the depth of tumor invasion at different stages of progression. This nonlinear photonic tomography method may help physicians to evaluate noninvasively the state of tissues *in vitro* and *in vivo*.

The authors thank Dr. A. Katz and Dr. S. Gayen for helpful discussion and technical help in computer programming; Dr. N. Zhadin for his assistance in computer programming; and Dr. Bing Xu for technical help with the laser system. This research is supported in part by Department of Energy Center of Excellence program, Medi-science Technology Corp., New York State Science and Technology Foundation, and Air Force Office of Scientific Research.

1. Fine, S. & Hansen, W. P. (1971) *Appl. Opt.* **10,** 2350–2353.
2. Sheppard, C. J. R., Gannaway, J. N., Kompfer, R. & Walsh, D. (1977) *IEEE J. Quant. Electron.* **13,** 100D (abstr.).
3. Freund, I., Deutch, M. & Sprecher, A. (1986) *Biophys. J.* **50,** 693–712.
4. Shen, Y. R. (1984) *Principles of Nonlinear Optics* (Wiley, New York).
5. Heinz, T. F., Chen, C. K., Richard, D. & Shen, Y. R. (1982) *Phys. Rev. Lett.* **48,** 478–481.
6. Guo, Y., Ho, P. P., Savage, H., Harris, D., Sacks, P., Schantz, S., Liu, Feng, Zhadin, N. & Alfano, R. R. (1997) *Opt. Lett.* **22,** 1323–1325.
7. Huang, D., Swanson, E. A., Lin, C. P., Schuman, J., S., Stinson, W. G., Chang, W., Hee, M., R., Flotte, T., Gregory, K., Puliafito, C. A., *et al.* (1991) *Science*, **254**, 1178–1181.
8. Pawley, J. B., ed. (1995) *Handbook of Biological Confocal Microscopy* (Plenum, New York), 2nd Ed.
9. Fenster, A. & Downey, D. R. (1996) *IEEE Eng. Med. Biol.* **15,** 41–51.
10. Salley, J. J. (1954) *J. Dent. Res.* **33,** 253–262.
11. Cheong, W., Prahl, S. A. & Welch, A. J. (1990) *IEEE J. Quant. Electron.* **26,** 2166–2185.
12. Ying, J., Liu, F. & Alfano, R. R. (1999) *Appl. Opt.* **38,** 224–229.